Disorder effects in diluted magnetic semiconductors

Carsten Timm and Felix von Oppen

Institut für Theoretische Physik, Freie Universität Berlin, Arnimallee 14, 14195 Berlin, Germany

Abstract. Diluted magnetic semiconductors (DMS) are promising materials for technological applications as well as interesting from the basic-physics point of view. It has become clear that disorder plays a crucial role in DMS due to the presence of many charged defects and the random positions of impurity spins. In this paper the effect of disorder on transport properties and magnetism in DMS is discussed. It is argued that the impurity positions are correlated due to strong Coulomb interactions between charged defects. These correlations are crucial for the understanding of magnetic properties and the observed metal-insulator transition.

The present interest in diluted magnetic semiconductors (DMS) has been fueled by possible applications in *spintronics* [1]. Particularly promising are ferromagnetic DMS produced by heavily doping technologically relevant semiconductors with transition-metal ions such as manganese. These materials are also fascinating from the basic-physics point of view. They combine strong electronic correlations in the d-shells, unusual transport properties, and strong disorder effects. In this paper we focus on the effects of disorder on transport and magnetism in Mn-doped GaAs. Disorder is expected to be strong due to the presence of a high concentration of charged impurities; the typical distance between these defects is roughly of the same order as the Fermi wave length. See Ref. [2] for a recent review on disorder in DMS.

In (Ga,Mn)As, substitutional Mn both acts as an acceptor and provides a localized spin $S = 5/2$ due to its half-filled d-shell. The doped hole is weakly bound to the acceptor by Coulomb attraction, forming a hydrogenic impurity state split off from the valence band [3,4]. The local impurity spin is coupled to the valence-band holes by exchange interaction. The shallow-impurity description probably applies since states dominated by Mn d-orbitals are far from the Fermi energy [3–5].

Because of the low Mn solvability, $Ga_{1-x}Mn_xAs$ has to be grown by low-temperature molecular beam epitaxy (MBE) at about 250°C. Homogeneous growth with up to $x \approx 0.08$ has been achieved. Ferromagnetic order has first been found by Ohno *et al.* [6]. Recently Curie temperatures above 160 K have been reached due to improved control over the defect concentrations [7,8].

Since Mn is an acceptor, (Ga,Mn)As is of p-type. However, the observed hole concentration is lower than the concentration of acceptors due to compensation, probably by arsenic antisites (As at cation sites) and Mn interstitials. Both types of defects are *double donors*. Antisites are expected for

low-temperature growth [9]. A high concentration of Mn is believed to lead to increased incorporation of the oppositely charged antisites [10–12]. When As_4 quadrumers are cracked before they arrive at the surface, the antisite concentration can be strongly reduced [13,7,8]. The presence of Mn interstitials has been proposed in Ref. [14] and demonstrated in channelling Rutherford backscattering experiments by Yu *et al.* [15], where about 17% of Mn impurities have been found in interstitial positions.

The ferromagnetic interaction between the impurity spins is carrier-mediated, as demonstrated by electric field-effect experiments [17–19]. On the other hand, in (Ga,Mn)As a metal-insulator transition between ferromagnetic *insulating* samples with small Mn concentration x and ferromagnetic *metallic* samples with larger x is observed [9,16]. Even for the most metallic samples the resistivity is relatively high, of the order of 10^{-3} to $10^{-2}\,\Omega\,\mathrm{cm}$ [9,20,13], showing that disorder is rather strong even in this regime.

This paper gives arguments why the defects are present in correlated, not random, positions [11,21,2]. In Sec. 1 Monte Carlo (MC) simulations are used to support this proposition. In Secs. 2 and 3 we show that the experimental results for transport and magnetic properties can only be understood assuming such correlations.

1 Defect Positions, Growth, and Annealing

In the present section we consider the spatial distribution of defects, i.e., substitutional Mn, As antisites, and interstitial Mn. We explain why the defect positions should be strongly correlated. We employ a rather simple model, which focuses on the screened Coulomb interaction between charged defects. For small defect separations other contributions to the interaction also become relevant. Ab-initio calculations for defect clusters [22–25] can be used to gain information on these "chemical" contributions. However, our conclusions are unaffected by the specific form of the short-range interaction.

In heavily compensated DMS the electronic screening of the Coulomb interaction between charged defects is rather weak [26]. Therefore, the electronic screening length is large compared to the typical separation between defects. This should lead to two effects [11,21,2]: Firstly, during growth defects of the same (opposite) charge are predominantly incorporated with larger (smaller) separations. Secondly, upon annealing defects further reduce their Coulomb energy through defect diffusion. There is another important effect relevant during annealing: Mn interstitials are more mobile than the other defects [15] due to lower energy barriers for their motion. Conversely, antisites are believed to be rather immobile at typical annealing temperatures (250°C) [27]. During annealing interstitial Mn seems to diffuse out of the bulk to the free surface of the DMS film [28]. Experiments show that capping of a (Ga,Mn)As film with GaAs suppresses the annealing effects [28]. This suggests that the annealing dependence of physical quantitites of these

high-quality samples is dominated by out-diffusion of interstitials and not by redistribution of defects within the bulk.

1.1 Defect Clusters

We first consider a simplified model where the compensation is assumed to be completely due to antisites. We start from a random distribution of Mn impurities and antisites on the cation sublattice, where the density of antisites is determined by charge neutrality from the observed hole concentrations. The Hamiltonian reads

$$H = \frac{1}{2} \sum_{i,j} \frac{q_i q_j}{\epsilon r_{ij}} e^{-r_{ij}/r_{\rm scr}}, \tag{1}$$

where q_i are the defect charges and r_{ij} is their separation. Relative to the cation sublattice, Mn impurities (antisites) carry charge $q = -1$ $(+2)$. The screening length $r_{\rm scr}$ is obtained from nonlinear screening theory [26]; it hardly affects the small-scale defect correlations. We perform MC simulations for the Hamiltonian H at the growth/annealing temperature 250°C for systems of $20 \times 20 \times 20$ conventional face-centered-cubic (fcc) unit cells with periodic boundary conditions, unless stated otherwise. The simulation is terminated when the spatial correlation function of the Coulomb potential (discussed below) does not change anymore.

As an illustration, Fig. 1 shows an equilibrated configuration of defects for Mn concentration $x = 0.05$ and $p = 0.3$ holes per Mn. Both substitutional Mn and antisites have been assumed to be mobile. This plot is for a supercell size of $10 \times 10 \times 10$ to make it more clear. It is obvious that the defects form small clusters, where typically an antisites is surrounded by several Mn impurities. The clustering leads to a strongly reduced Coulomb energy.

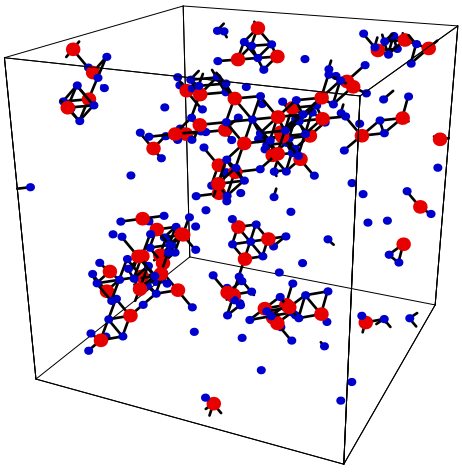

Fig. 1. Equilibrated configuration of defects on a $10 \times 10 \times 10$ lattice for Mn concentration $x = 0.05$ and $p = 0.3$ holes per Mn. The host lattice is not shown. Small dark circles denote Mn impurities, whereas large circles are As antisites. Solid bars connect defects on nearest-neighbor sites.

Before we turn to a quantitative analysis of the MC results, we consider what happens if we do not start from a random configuration. This is motivated by experiments on *digital heterostructures* consisting of half monolayers of MnAs separated by thick layers of GaAs [29]. All samples are insulating for $T \to 0$ [29]. Part of the Mn apparently diffuses out of the MnAs layers [29]. We have performed MC simulations for a superlattice of single layers with half the Ga replaced by Mn separated by low-temperature GaAs with 0.25% antisites. The superlattice period is 20 fcc unit cells. Figure 2 shows the configuration when some interdiffusion has occured.

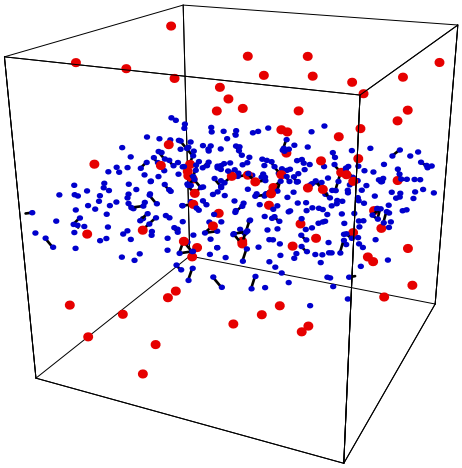

Fig. 2. Configuration of defects for a superlattice of half monolayers of MnAs between thick layers of low-temperature GaAs. A supercell of $20 \times 20 \times 20$ fcc unit cells has been used. 2000 MC steps have been performed, leading to interdiffusion of Mn into the GaAs layers. The configuration is still far from equilibrium.

It is known that a significant fraction of Mn forms interstitials [15]. There are two relevant non-equivalent interstitial positions, namely positions coordinated by four As or by four Ga ions [30]. Ab-initio calculations indicate that the As-coordinated T(As_4) position is lower in energy by 0.3 to 0.35 eV compared to the Ga-coordinated position [8,31]. We have performed MC simulations including charged ($q = +2$) interstitials and assuming the onsite energy in the T(As_4) position to be 0.3 eV lower [2]. Figure 3 shows an equilibrated configuration for a concentration of *substitutional* Mn of $x = 0.05$ as above, but concentrations of 0.005 of antisites and 0.0125 of Mn interstitials. This corresponds to the same hole concentration as in Fig. 1. All defects have been assumed to be mobile. Again, the defects form small clusters.

1.2 Disorder Potential

The cluster formation can be discussed quantitatively by introducing the correlation function $D(r)$ of the disorder potential $V(\mathbf{r})$:

$$D(r) \equiv \langle V(\mathbf{r})\, V(\mathbf{r}')\rangle_{|\mathbf{r}-\mathbf{r}'|=r} - \langle V\rangle^2. \tag{2}$$

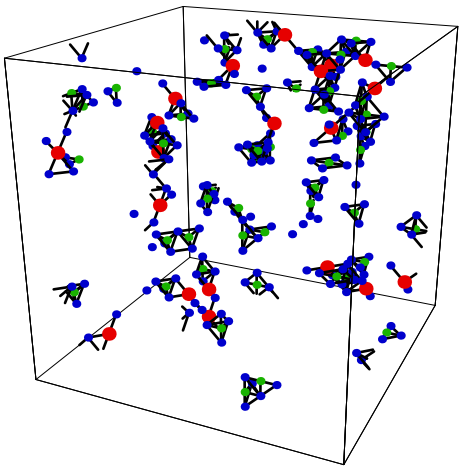

Fig. 3. Equilibrated configuration of defects on a $10 \times 10 \times 10$ lattice for substitutional Mn concentration $x = 0.05$ and $p = 0.3$ holes per substitutional Mn. This requires a concentration of 0.0175 of compensating double donors, which are assumed to be antisites with a concentration of 0.005 and Mn interstitials (small light circles) with a concentration of 0.0125.

$V(\mathbf{r})$ is a sum over screened Coulomb potentials from all impurities. This potential determines the localization properties of the valence-band holes. Obviously, $\Delta V \equiv \sqrt{D(0)}$ is the *width* of the distribution of $V(\mathbf{r})$. Figure 4 shows $D(r)$ for various assumptions on the type and mobility of defects. The equilibration strongly reduces $D(r)$ and ΔV in all cases. However, ΔV is still *not* small compared to the Fermi energy so that disorder cannot be neglected [11,2]. Without interstitials (cf. Fig. 1) the disorder potential becomes short-range correlated. In equilibrium $D(r)$ decays on the scale of the nearest-neighbor separation due to the screening of the *compensated* Mn impurities [21,2]. The remaining uncompensated Mn ions cannot be screened by antisites and their contribution decays on a longer length scale determined by their density. Assuming antisites to be immobile [27] has practically no effect.

The interstitials do not change the qualitative picture. $D(r)$ still decays on the length scale of the nearest-neighbor separation. This result changes only weakly if we assume the two different interstitial sites to have the same energy since the energy difference of 0.3 eV is unimportant compared to the Coulomb energy. Again, it makes no difference if the antisites are treated as immobile. The short-range correlations of $V(\mathbf{r})$ simplify transport calculations [32]. However, if we also assume the *substitutional* Mn to be immobile, the absolute value and the width of the correlation function drastically increase. In this case the small concentration of Mn interstitials cannot effectively screen the Mn substitutionals.

The scenario of immobile substitutionals agrees with the suggestion that annealing mostly leads to outdiffusion of interstitials and not to redistribution of substitutional defects [28]. In this case defect correlations are expected to develop mainly during growth. We argue in the following that they have to be present to explain the observations. On the other hand, the experiments on digital heterostructures [29] would be hard to interpret if substitutional

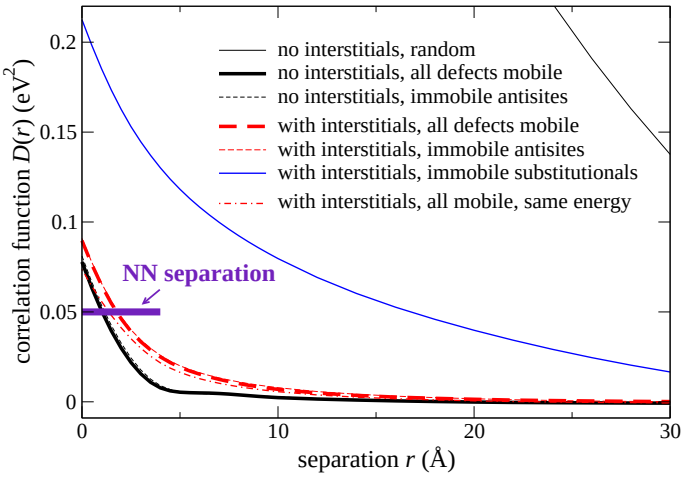

Fig. 4. Correlation function $D(r)$ of the disorder potential for a $20 \times 20 \times 20$ supercell. A concentration $x = 0.05$ of substitutial Mn and $p = 0.3$ holes per substitutional Mn have been assumed. The thin solid line lying mostly outsite the scope of the figure shows the result for a random distribution of defects (in this case without interstitials). The other curves show $D(r)$ for equilibrated configurations with or without interstitials under various assumptions on the mobility of different defect species as given in the legend. The heavy horizontal bar denotes the nearest-neighbor separation on the cation sublattice.

Mn were totally immobile. The observed interdiffusion of Mn would require a probably unrealistically high fraction of interstitial Mn. The presence of cation vacancies could make substitutional defects more mobile [20].

We note that in Ref. [25] small clusters of three Mn defects are studied within density-functional theory. Clusters made up of two substitutional and one interstitial defects are found to be favored due to their Coulomb attraction, in agreement with the above discussion. As noted above, ab-initio theory captures additional contributions to the energy not included here.

2 Hole states

Next, we consider the properties of the valence-band holes subjected to the impurity potential $V(\mathbf{r})$. In particular, we are interested in their spectrum and localization properties. To exhibit the main physics we again employ a simple model, which consists of the envelope-function and parabolic-band approximations and starts from the single-hole Hamiltonian

$$H = -\frac{\hbar^2}{2m^*}\nabla^2 + V(\mathbf{r}). \tag{3}$$

The hole Hamiltonian diagonalized numerically in a plane-wave basis [11]. The calculations are done for spin-less holes, since the additional disorder

introduced by the exchange interaction is found to be small. We reintroduce the exchange below. The diagonalization yields the energy spectrum and eigenfunctions $\psi_n(\mathbf{r})$, from which we calculate the participation ratios

$$\mathrm{PR}(n) = \frac{\left[\sum_{\mathbf{r}} |\psi_n(\mathbf{r})|^2\right]^2}{\sum_{\mathbf{r}} |\psi_n(\mathbf{r})|^4}. \tag{4}$$

The PR allows to estimate the position of the mobility edge in the valence band since it scales with system size for extended states but essentially remains constant for localized states.

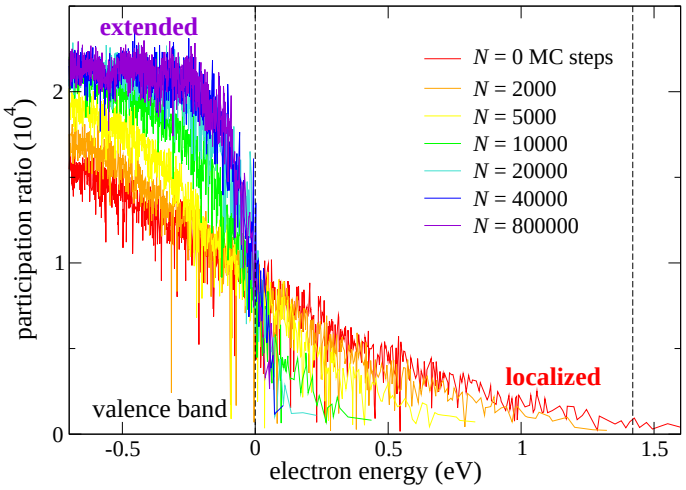

Fig. 5. Participation ratio as a function of energy for $x = 0.05$ and $p = 0.3$ after various numbers N of MC steps increasing from the flattest to the steepest curve. The unperturbed band edges are marked by vertical dashed lines.

Figure 5 shows the PR as a function of energy for a Mn concentration of $x = 0.05$ and $p = 0.3$ holes per Mn [9], for various numbers of MC steps, N [2]. For fully random defects ($N = 0$) the valence-band edge is smeared by disorder to such an extent that the gap becomes filled, in contradiction to experiments. On the other hand, after equilibration only very few states remain in the gap. Thus the defect clustering is *required* to explain the persistence of the gap. From finite-size scaling results (not shown) we know that the PR in the flat region and the upper part of the slope scales with system size, whereas it becomes independent of system size in the band tail [11,21]. The mobility edge thus lies on the slope in Fig. 5. Due to numerical constraints the finite-size scaling could not be extended to large enough systems to pinpoint the mobility edge exactly.

Transport properties are dominated by the states close to the Fermi energy E_F. To find E_F one has to take the splitting of the valence band by the

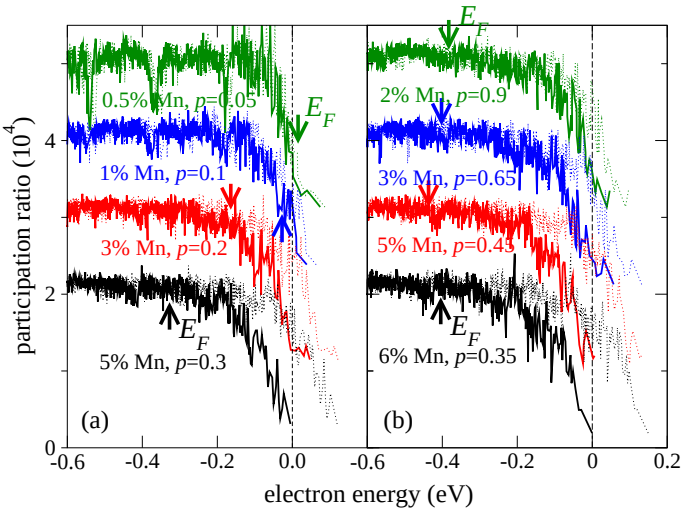

Fig. 6. Participation ratio for equilibrated configurations as a function of energy for various parameters x and p given in the plot, (a) for the (Ga,Mn)As samples of [9], (b) for the samples of [13]. For the exchange splitting of the band full magnetization of Mn spins has been assumed. The Fermi energy is in each case indicated by an arrow.

exchange interaction into account. As noted above, the disorder due to this interaction is small. However, its *average* is not negligible. Figure 6 shows the PR as a function of energy for parameters appropriate for (a) the samples meassured by Matsukura, Ohno *et al.* [9] and (b) the samples of Edmonds *et al.* [13]. The defect concentration has relatively little effect on the PR curve due to the strong ionic screening. In (a) the main effect is the shift of the Fermi energy due to the strongly changing hole concentration. The states at the Fermi energy are extended for $x \geq 0.03$, while they are localized for $x = 0.005$ [11,2], in reasonable agreement with the experimentally observed metal-insulator transition [9]. On the other hand, in (b) the Fermi energy hardly changes at all and stays well in the extended region, consistent with the experimental observation of metallic transport from $x = 0.0165$ to $x = 0.088$ in these samples [13,33]. The growth technique of Ref. [13] leads to very low compensation at small Mn concentrations and to *increasing* compensation with increasing Mn doping, oppositely to what is observed in Refs. [9].

For fully random defects the states at the Fermi energy would in all cases show a strong tendency towards localization. Thus cluster formation is required to understand why (Ga,Mn)As becomes metallic at all.

Finally, we show in Fig. 7 the PR for the simulation starting from a half layer of MnAs between thick layers of low-temperature GaAs, see Fig. 2. The broadening of the band due to disorder is very strong for weak interdiffusion ($N = 2000$) and the PR is strongly reduced. This strong tendency towards

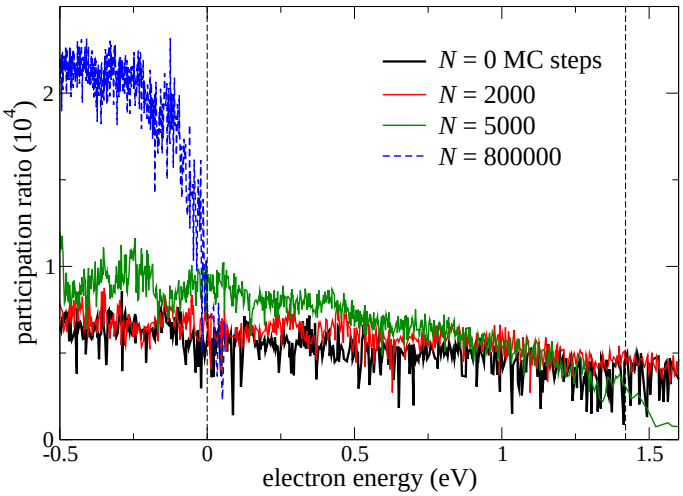

Fig. 7. Participation ratio as a function of electron energy for a superlattice of half monolayers of MnAs between thick layers of low-temperature GaAs, see Fig. 2, for various numbers of MC steps.

localization is in agreement with experiments [29]. Ionic screening is rather inefficient since the Mn defects and the oppositely charged antisites first have to come close together to form clusters. The PR curve for $N = 800000$ shows that eventually states close to equilibrium are reached.

3 Magnetic order

So far, we have only included the exchange interaction with the Mn impurities through a homogeneous exchange field, i.e., at the level of the virtual crystal approximation (VCA) [34]. We now study the magnetic order within a selfconsitent mean-field approximation, which, importantly, fully includes the disorder [11,2]. We start from a Zener model with the Hamiltonian

$$H = \sum_{n\sigma} \xi_n \, c^\dagger_{n\sigma} c_{n\sigma} - J_{\rm pd} \sum_i \mathbf{s}_i \cdot \mathbf{S}_i, \tag{5}$$

where the $\mathbf{S}_i$ are Mn spins ($S = 5/2$) and

$$\mathbf{s}_i \equiv \sum_{n\sigma n'\sigma'} c^\dagger_{n\sigma} \psi^*_n(\mathbf{R}_i) \, \frac{\boldsymbol{\sigma}_{\sigma\sigma'}}{2} \, \psi_{n'}(\mathbf{R}_i) c_{n'\sigma'} \tag{6}$$

are hole-spin polarizations at the Mn sites. ξ_n and ψ_n are the hole eigenenergies and eigenfunctions, respectively, for vanishing magnetic interaction obtained in the previous section. Note that H contains the full Coulomb disorder potential. ξ_n includes the chemical potential. The antiferromagnetic exchange interaction is assumed to be local. In a more realistic model one should take its

nonzero range into account, which stems from the hybridization between Mn d-orbitals and As p-orbitals. The finite range is important for the anisotropy of the effective exchange interaction between impurity spins [35].

The Hamiltonian (5) is decoupled in a mean-field approximation without taking a spatial average [11,21,2]. At each impurity site the product $\mathbf{s}_i \cdot \mathbf{S}_i$ is replaced by $\langle \mathbf{s}_i \rangle \cdot \mathbf{S}_i + \mathbf{s}_i \cdot \langle \mathbf{S}_i \rangle - \langle \mathbf{s}_i \rangle \cdot \langle \mathbf{S}_i \rangle$. The averaged hole spins $\langle \mathbf{s}_i \rangle$ are expressed in terms of the mean-field Zeeman splittings of the hole states n. This leads to a large set of coupled mean-field equations which are solved numerically. A collinear magnetization is assumed. One can show that the equation for the Curie temperature T_c, obtained by linearizing the mean-field equations, is unchanged by dropping this assumption.

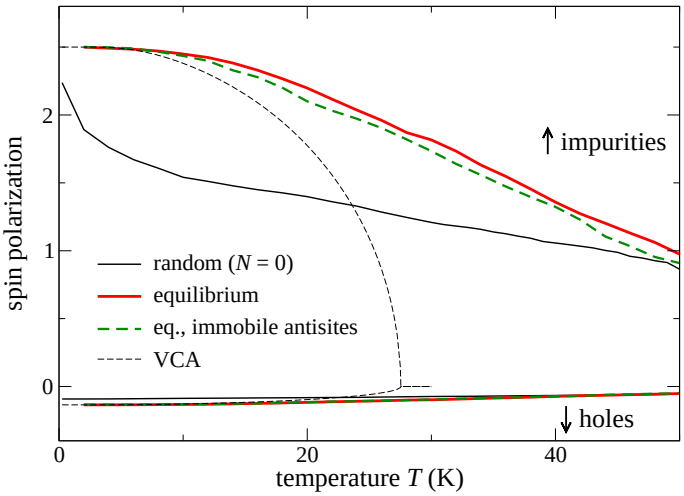

Fig. 8. Spin polarization of Mn spins (up) and hole spins (down) as functions of temperature for $x = 0.05$ and $p = 0.3$ for random and equilibrated/clustered configurations. The spin polarization for an equilibrated system with immobile antisites is also shown. For comparison, the curves labeled by "VCA" show the magnetizations obtained from a theory that totally neglects disorder.

Figure 8 shows the magnetization curves for Mn and hole spins for $x = 0.05$ and $p = 0.3$ for random and equilibrium defect configurations, assuming compensation by antisites [11,21,2]. Since these results are obtained from mean-field theory, they are most reliable at low temperatures. However, it has been suggested that mean-field theory is quite good for metallic (Ga,Mn)As in the whole temperature range [36,37,34]. The Mn magnetization curve shows *upwards* curvature for random defects. Similar magnetization curves have been calculated by many different approaches, see Ref. [2]. This general shape seems to be a robust feature of highly disordered ferromagnets. Within mean-field theory, the anomalous shape is due to the localization tendency of the

holes, which leads to a shorter-range effective Mn-Mn spin interaction and thus to a broader distribution of effective fields acting on these spins.

For the clustered configuration the magnetization curve shows *downward* curvature and is more Brillouin-function-like at low temperatures. The crossover from upward to downward curvature agrees qualitatively with experimental annealing studies [20]. Conversely, the assumption of clustered defects is crucial to understand the downward curvature observed for optimally annealed samples. Figure 8 also shows that assuming immobile antisites again does not have a strong effect. Neglecting the disorder by setting $V(\mathbf{r}) = 0$ and replacing the Mn spins by a homogeneous spin density (VCA) leads to a strongly reduced Curie temperature. This may be an artifact of mean-field theory, but since the impurity-spin polarization exceeds the VCA result even at the lowest temperatures, where mean-field theory should be valid, we suggest that disorder indeed has the tendency to stabilize ferromagnetism.

We do not expect Mn interstitials to change this picture qualitatively. Manganese impurities in adjacent substitutional and interstitial positions should interact antiferromagnetically due to superexchange. The strength of this interaction is at least -26 meV [30], leading to the formation of spin singlets that do not participate in ferromagnetic order. This suggests to take only the substitutionals into account that are not paired up in singlets.

4 Summary

Correlated defect clusters develop naturally in DMS due to the strong Coulomb interactions between oppositely charged defects. The clustering is expected to take place during growth or annealing and leads to a strongly reduced impurity potential. This effect is necessary to explain the experimental observations regarding the metal-insulator transition as a function of Mn doping and the persistence of the semiconductor gap. We also find that the magnetization curve crosses over from an anomalous shape to a more Brillouin-function-like dependence, in agreement with experiments. In high-quality samples the cluster formation has to take place already during growth since they already show metallic behavior and convex magnetization curves *as grown* [28]. While the simple model employed in this study precludes quantitative comparison with experiments, the general conclusions do not depend on model details.

5 Acknowledgements

Part of the results have been obtained in collaboration with F. Höfling and F. Schäfer. We thank T. Dietl, S.C. Erwin, G.A. Fiete, P. Kacman, A.H. MacDonald, M.E. Raikh, J. Sinova, and G. Zaránd for helpful discussions.

References

1. S.A. Wolf *et al.*: Science **294**, 1488 (2001)
2. C. Timm: J. Phys.: Condensed Matter **15**, R1865 (2003)
3. M. Linnarsson *et al.*: Phys. Rev. B **55**, 6938 (1997)
4. J. Okayabashi *et al.*: Phys. Rev. B **58**, R4211 (1998)
5. T. Dietl: Semicond. Sci. Technol. **17**, 377 (2002)
6. H. Ohno *et al.*: Appl. Phys. Lett. **69**, 363 (1996)
7. K.C. Ku *et al.*: Appl. Phys. Lett. **82** 2302 (2003)
8. K.W. Edmonds *et al.*: Phys. Rev. Lett. **92**, 037201 (2004)
9. F. Matsukura, H. Ohno, A. Shen, Y. Sugawara: Phys. Rev. B **57**, R2037 (1998)
   H. Ohno: Science **281**, 951 (1998)
   H. Ohno: J. Magn. Magn. Mat. **200**, 110 (1999)
10. B. Grandidier *et al.*: Appl. Phys. Lett. **77**, 4001 (2000)
11. C. Timm, F. Schäfer, F. von Oppen: Phys. Rev. Lett. **89**, 137201 (2002)
12. L. Bergqvist *et al.*: Phys. Rev. B **67**, 205201 (2003)
13. K.W. Edmonds *et al.*: Appl. Phys. Lett. **81**, 3010 (2002)
14. J. Mašek, F. Máca: Acta Phys. Pol. A **100**, 319 (2001)
15. K.M. Yu *et al.*: Phys. Rev. B **65**, 201303(R) (2002)
16. H. Ohno, F. Matsukura: Sol. State Commun. **117**, 179 (2001)
17. H. Ohno *et al.*: Nature **408**, 944 (2000)
18. D. Chiba, M. Yamanouchi, F. Matsukura, H. Ohno: Science **301**, 943 (2003)
19. A.M. Nazmul, S. Kobayashi, S. Sugahara, M. Tanaka: cond-mat/0309532 (2003)
20. S.J. Potashnik *et al.*: Appl. Phys. Lett. **79**, 1495 (2001)
21. C. Timm, F. von Oppen: J. Supercond. **16**, 23 (2003)
22. M. van Schilfgaarde, O.N. Mryasov: Phys. Rev. B **63**, 233205 (2001)
23. H. Raebiger, A. Ayuela, R.M. Nieminen: cond-mat/0307364 (2003)
24. J.M. Sullivan *et al.*: Phys. Rev. B **68**, 235324 (2003)
25. P. Mahadevan, A. Zunger: cond-mat/0309502 (2003)
26. B.I. Shklovskii, A.L. Efros: *Electronic Properties of Doped Semiconductors* (Springer-Verlag, Berlin 1984)
27. M. Suezawa: *Int. Conf. on Science and Technology of Defect Control in Semiconductors* (Yokohama, Japan), vol. II, K. Sumino (Ed.) (North Holland, Amsterdam 1990), p. 1043
28. M.B. Stone *et al.*: Appl. Phys. Lett. **83**, 4568 (2003)
29. R.K. Kawakami *et al.*: Appl. Phys. Lett. **77**, 2379 (2000)
    E. Johnston-Halperin *et al.*: Phys. Rev. B **68**, 165328 (2003)
30. J. Mašek, F. Máca: cond-mat/0308568 (2003)
31. J.M. Sullivan, S.C. Erwin: unpublished (2003)
32. C. Timm, F. von Oppen, F. Höfling: Phys. Rev. B (in press), cond-mat/0309547 (2003)
33. B.L. Gallagher: private communication (2003)
34. J. König, J. Schliemann, T. Jungwirth, A.H. MacDonald: *Electronic Structure and Magnetism of Complex Materials, Springer Series in Material Sciences*, vol. **54**, D.J. Singh and D.A. Papaconstantopoulos (Eds.) (Springer-Verlag, Berlin 2003), pp. 163–211
35. C. Timm, A.H. MacDonald: unpublished (2004)
36. T. Dietl *et al.*: Science **287**, 1019 (2000)
37. T. Jungwirth *et al.*: Appl. Phys. Lett. **81**, 4029 (2002)
    T. Jungwirth *et al.*: Appl. Phys. Lett. **83**, 320 (2003)